Published in final edited form as:

Drug Dev Ind Pharm. 2016 ; 42(3): 485–496. doi:10.3109/03639045.2015.1104347.

Solid-state Characterization of Felodipine-Soluplus® Amorphous Solid Dispersions

Jiannan Lu[1,2], **Kristina Cuellar**[3], **Nathan I. Hammer**[3], **Seongbong Jo**[1], **Andreas Gryczke**[4], **Karl Kolter**[5], **Nigel Langley**[6], and **Michael A. Repka**[1,7,*]

[1]Department of Pharmaceutics and Drug Delivery, School of Pharmacy, the University of Mississippi, University, MS 38677, USA

[3]Department of Chemistry and Biochemistry, the University of Mississippi, University, MS 38677, USA

[4]BASF SE, Global Development and Technical Marketing, Ludwigshafen, Germany

[5]BASF SE, R&D Product Management Excipients, Ludwigshafen, Germany

[6]BASF Corporation, Tarrytown, NY, USA

[7]Pii Center for Pharmaceutical Technology, School of Pharmacy, the University of Mississippi, University, MS 38677, USA

Abstract

The aim of the current study is to develop amorphous solid dispersion via hot melt extrusion technology to improve the solubility of a water-insoluble compound, felodipine. The solubility was dramatically increased by preparation of amorphous solid dispersions via hot-melt extrusion with an amphiphilic polymer, Soluplus®. Felodipine was found to be miscible with Soluplus® by calculating the solubility parameters. The solubility of felodipine within Soluplus® was determined to be in the range of 6.2–9.9% (w/w). Various techniques were applied to characterize the solid-state properties of the amorphous solid dispersions. These included Fourier Transform Infrared Spectroscopy and Raman spectroscopy to detect the formation of hydrogen bonding between the drug and the polymer. Scanning electron microscopy was performed to study the morphology of the solid dispersions. Among all the hot-melt extrudates, felodipine was found to be molecularly dispersed within the polymer matrix for the extrudates containing 10% drug, while few s mall crystals were detected in the 30 and 50% extrudates. In conclusion, solubility of felodipine was enhanced while a homogeneous solid dispersion was achieved for 10% drug loading.

Keywords

felodipine; amorphous solid dispersion; solid-state characterization; hot-melt extrusion; miscibility/solubility

*Address for correspondence: Michael A. Repka, Ph.D., Professor and Chair, Department of Pharmaceutics and Drug Delivery, Pii Center for Pharmaceutical Technology, School of Pharmacy, The University of Mississippi, University, MS 38677, Phone: 662-915-1155, Fax: 662-915-1177, marepka@olemiss.edu.

[2]Current address: Pharmaceutical Application Laboratory, Shin-Etsu Chemical, Co. Ltd., Totowa, NJ 07512, USA

Introduction

Sufficient aqueous solubility is one of the necessities for oral absorption of a drug. Limited solubility can delay the dissolution and further reduce the bioavailability of a drug [1]. As a result, great efforts have been made to address this issue. Amorphous solid dispersions have been widely explored to increase the solubility and bioavailability of sparingly water-soluble compounds[2-6]. It has been proven that amorphous compounds can demonstrate solubility and dissolution rates several times higher than those demonstrated by their crystalline forms. However, amorphous substances are usually thermodynamically metastable and have a tendency to undergo phase separation or recrystallization during storage. Moreover, a solution-mediated phase transformation is often observed during the dissolution process[7, 8]. Supersaturation is the driving force for the phase transformation; hence, once subjected to the dissolution medium, metastable solids tend to precipitate via a nucleation and crystal growth pathway[9, 10]. Various kinds of pharmaceutical excipients are investigated in order to extend the supersaturation time and a direct excipient–drug interaction, such as hydrogen bonding, is believed to contribute to the stabilization effect[2, 11-16].

Numerous approaches have been utilized to prepare solid dispersions. Among them is hot melt extrusion, which is receiving increasing attention owing to its unique advantages over other techniques[17-22]. Beyond its tremendous capability for solubility/bioavailability enhancement and industrial scalability, it is a continuous process with a limited number of steps and is cost-effective; in addition, the absence of organic solvents in the overall process makes this technique environment-friendly[17].

The solubility parameter δ can be used to quantify the cohesive energy, which represents the strength of attraction between constituent molecules in a substance. In other words, δ determines the energy input required to remove one molecule from its adjacent molecule to an infinite distance, from a thermodynamic standpoint[23-25]. All kinds of intermolecular interactions, including Van der Waals, covalent bonding, hydrogen bonding, and ionic and electrostatic interactions, contribute to the cohesive energy [23]. Solubility parameter has been broadly applied to estimate the likelihood of drug–polymer miscibility [26-29] since it was first introduced by Hildebrand [30]. The solubility parameter was initially defined as [30]:

$$\delta=\left(\frac{E_T}{V}\right)^{1/2} \quad (1)$$

Where E_T is the cohesive energy and V is the molar volume.

It was pointed out by Hansen that not only the contribution from dispersion forces E_d, but also those from the polar forces E_p and the hydrogen bonding E_h should be considered when predicting the cohesive energy of substances [31]. Hence, the overall cohesive energy can be written as:

$$E_T=E_d+E_p+E_h \quad (2)$$

The solubility parameter can be further expressed as:

$$\delta_T^2=\delta_d^2+\delta_p^2+\delta_h^2 \quad (3)$$

Two group contribution methods, the Hoy method and the Hoftyzer–Van Krevelen method, were developed to determine the solubility parameter, based on Hansen's assumption [32, 33].

In the Hoy method, for low molecular weight substances:

$$\delta_T=(F_i+B)/\mathrm{V} \quad (4)$$

and for amorphous polymers:

$$\delta_T=(F_i+B/N)/\mathrm{V} \quad (5)$$

where F_i is the summary of molar attraction of each component in the structure; B, as a constant, is the base value; and N is the number of repeating units in each effective chain, which can be calculated as:

$$N=0.5/\Delta_T^{(P)} \quad (6)$$

where Δ_T is the Lydersen correction for non-ideality.

In the Hoftyzer–Van Krevelen method:

$$\delta_d=\frac{\sum F_{di}}{V},\ \delta_p=\frac{\sqrt{\sum F_{pi}^2}}{V},\ \delta_h=\sqrt{\frac{\sum E_{hi}}{V}} \quad (7)$$

where, F_{di} is molar attraction constant of dispersion, F_{pi} is dipole-dipole interactions and E_{hi} is hydrogen bonding contribution in the chemical structure [24].

In the present study, the effectiveness of Soluplus® (SOL) as an appropriate excipient to improve the aqueous solubility of a poorly water-soluble compound, felodipine (FEL), was evaluated. FEL-SOL solid dispersions containing 10, 30, and 50% FEL were prepared via hot-melt extrusion and subjected to further studies. In order to understand the solid-state properties of the solid dispersions, various techniques were utilized in this study.

Materials and Methods

Materials

FEL (figure 1a), a long-acting 1,4-dihydropyridine-calcium channel blocker with poor aqueous solubility (less than 1 mg/L at 37°C), was purchased from Ria International LLC

(East Hanover, NJ, USA). SOL (figure 1b), a graft amorphous polymer with a low glass transition temperature (approximately 70°C), was kindly donated by BASF SE (Ludwigshafen, Germany). Sodium hydroxide and monobasic potassium phosphate were purchased from Sigma-Aldrich (St. Louis, MO, USA). All the organic solvents and water were of high-performance liquid chromatography (HPLC) grade.

Solubility Parameter Calculation

The solubility parameter δ was calculated using the Hoy and the Hoftyzer–Van Krevelen methods, and the average value from the two methods was used to estimate the drug–polymer miscibility as recommended since both methods provide the same accuracy level (10%) [24]. To determine the solubility parameter for SOL, which is composed of polyvinyl caprolactam (PVC): polyvinyl acetate (PVA): polyethylene glycol (PEG) at a ratio of 57:30:13, the number average of the three monomers was calculated.

Differential Scanning Calorimetry

The solubility of FEL in SOL matrix was predicted by using a Perkin-Elmer Diamond differential scanning calorimetry (DSC) instrument (Norwalk, CT, USA). Approximately 5–7 mg of binary physical mixtures of SOL with FEL ranging from 10 to 100% were weighed and sealed into an aluminum pan. The samples were heated from 30 to 180°C at various ramp rates of 10, 20, 50, and 100°C/min. The pure FEL heated at 10°C/min was also subjected to further treatments, as follows, to obtain the glass transition temperature: held at 180°C for 5 min, cooled down to 0°C at a rate of 100°C/min, and heated to 180°C again at the initial heating rate. The enthalpy of fusion of FEL was recorded and plotted versus the concentration. The extrudates were only subjected to a heating rate of 10°C/min. The instrument was calibrated with indium and zinc before carrying out the tests. Nitrogen was used as the purge gas at a flow rate of 20 mL/min. All the experiments were carried out in triplicate.

Hot-melt Extrusion

Physical mixtures containing 10, 30, and 50% FEL in batch sizes of 50 g were initially sieved with a USP 60 mesh and mixed in a V-cone blender (MaxiBlend™, GlobePharma, North Brunswick, NJ, USA) at 50 rpm for 15 min and further extruded with a co-rotating twin-screw extruder (16 mm Prism EuroLab, ThermoFisher Scientific, Stone, UK) into uniform rods at an extrusion temperature of 140°C and a screw speed of 100 rpm. Afterwards, part of each rod was milled into a fine powder using a laboratory grinder, and the rest was kept in a refrigerator at −4°C until further study.

Phase Solubility Determination

An excess amount of FEL (approximately 20 mg) was added to 20-mL vials containing either purified water or pH 6.8 phosphate buffer (with or without pre-dissolved SOL). The concentration of SOL varied from 0 to 1000 μg/mL (0, 10, 50, 100, 250, 500, and 1000 μg/mL). The samples were placed into a Precision Reciprocal Shaking Bath (ThermoFisher Scientific, Stone, UK) at 37°C and then shaken at 80 rpm for 24 hours to achieve equilibrium. Afterwards, the samples were filtered through a 0.45-μm nylon filter membrane

(Whatman, Piscataway, NJ, USA) and further analyzed by using HPLC with UV detection at a λ_{max} of 238 nm.

Particle Size Analysis

The samples from the phase solubility study were further subjected to particle size analysis using a Zetasizer Nano ZS Zen3600 (Malvern Instruments, Inc., Malvern, UK). The mean particle size and the polydispersity index were determined at 37°C with backscatter detection in disposable folded capillary clear cells. A 633-nm He–Ne laser was utilized to obtain the data, and the particle size analysis data were evaluated using volume distribution.

Drug Release Studies

All the extrudates were subjected to *in vitro* dissolution studies utilizing a Hanson SR8-plus™ dissolution test station (Hanson Research Corporation, Chatsworth, CA, USA) operated at a paddle speed of 100 rpm. The extrudates were weighed precisely to an amount containing 20 mg of FEL and filled into size #1 gelatin capsules. These capsules were placed in sinkers and added to the dissolution vessels. Two types of dissolution medium were utilized: 1) 500 mL of pH 6.8 phosphate buffer, and 2) 500 mL of pH 6.8 phosphate buffer with pre-dissolved SOL (250 and 500 μg/mL). Therefore, the theoretical maximum solubility of FEL is 40 μg/mL. At pre-determined time intervals, 1.5-mL samples were removed from the dissolution vessels and replaced with an equal volume of fresh dissolution medium. These collected samples were immediately filtered using 13-mm PTFE membrane filters (Whatman, Piscataway, NJ, USA) with a pore size of 0.2 μm and analyzed using HPLC with UV detection at a λ_{max} of 238 nm. All experiments were performed in triplicate and the mean values were compared.

Polarized Light Microscopy

The optical properties of pure FEL, SOL, and the extrudates were observed at room temperature using a Nikon Eclipse E600 Pol microscope equipped with a Nikon DS-Fi 1 camera. Images were analyzed using NIS-Elements BR 3.2 software. In addition, the extrudates were also exposed to a couple of droplets of dissolution medium (pH 6.8 phosphate buffer with or without pre-dissolved SOL), and observed under polarized light to understand the dissolution behavior.

FT-IR Spectroscopy

The FT-IR spectra of FEL, SOL, and the extrudates were obtained by using a PerkinElmer Spectrum 100 FT-IR Spectrometer, equipped with the universal ATR accessory, in the range of 4000–650 cm^{-1}, using a resolution of 1 cm^{-1}.

Raman Spectroscopy

The excitation sources employed for Raman spectroscopy were the 514.5 nm line and the 647 nm line from a Stabilite 2018 Kr/Ar mixed-gas ion laser. The spectra were collected in the range of 50–3600 cm^{-1} using a Jobin Yvon Ramanor HG2-S Raman spectrometer with two 1800 grooves/mm gratings and a thermoelectrically cooled (−30°C) photomultiplier

tube detector, as previously reported [34]. A scan speed of 2 cm^{-1}/s was employed. Spectra were obtained for solid-state FEL and SOL, as well as for the extrudates.

Theoretical Methods

Calculations were performed using the Gaussian 09 package (Revision A.1 ed.; Gaussian, Inc.: Wallingford, CT, USA, 2009). The optimized equilibrium geometry, vibrational frequencies, and Raman intensities of FEL were determined using the B3LYP density functional with the 6-311+g (d, p) basis set. Simulated spectra were constructed by using a custom program developed by National Instruments LabView, as previously reported [34].

X-ray Diffraction

X-ray diffraction (XRD) studies were performed on a powder X-ray diffraction apparatus (Bruker AXS, Madison, WI, USA) using CuKα radiation at 40 mA and 40 kV. The samples of interest were analyzed in the diffraction angles range of 5–35° (2θ) at a scan rate of 2°/min with a scanning step of 0.05°. All experiments were performed in triplicate.

Scanning Electron Microscopy

The morphology of the samples was determined by using a JEOL JSM-5600 scanning electron microscope at an accelerating voltage of 5 kV equipped with JSM 5000 software. Samples of interest were coated with gold by utilizing a Hummer 6.2 sputtering system for 10 min before observation.

Statistical Analysis

Analysis was performed using Microsoft Excel 2013 by a student's t-Test. Significance levels of $P < 0.05$ denoted significance in all cases.

Results and Discussion

It is crucial to measure the solubility/miscibility of drugs in polymers when developing amorphous solid dispersions since it will provide useful information regarding selection of the appropriate drug loading level along with prediction of the stability of solid dispersions [25]. Solubility is generally recognized as a thermodynamic parameter at which moment the chemical potential of the substance in the solvent equals the chemical potential of the substance precipitated, and the same concept can be used in drug–polymer systems [35]. The term miscibility was first introduced to polymer blends [36], and then further extrapolated to small-molecule systems. However, unlike polymer blends, amorphous drugs are usually metastable and tend to recrystallize, making it more complicated to predict the miscibility. As mentioned before, the solubility parameter was applied to predict the miscibility of FEL-SOL in the current study. The group contribution values of FEL and the three monomers of SOL are listed in Tables 1–8 [24]. Consequently, the solubility parameter for FEL was calculated as 20.78 and 22.74 according to the Hoy and the Hoftyzer/Van Krevelen methods, respectively. Meanwhile, the solubility parameter for SOL was determined as 21.49 and 21.79, respectively. The solubility parameter for SOL obtained by gas chromatography was 19.4 [37], which is close to the average value of 21.64 calculated in this study, indicating the accuracy of the methods used. As the predicted value from each method is well close, an

average value is acceptable here. It is well accepted that two substances are not miscible if the difference in their solubility parameters is larger than 10 $MP^{1/2}$ and good miscibility is expected when the difference is less than 7 $MP^{1/2}$, especially when the difference is less than 2 $MP^{1/2}$[28]. However, it is worth mentioning that solubility parameters only provide a simple theoretical pathway to predict the miscibility of drug–polymer systems from the initial assessment standpoint; it is always necessary to perform practical experiments to identify the miscibility of drug– polymer systems for formulation development. Nevertheless, we have clearly shown that the solubility parameters of FEL and SOL are very close to each other (Table 9), which indicates the likelihood of drug–polymer miscibility.

Figure 2a demonstrates the thermal behavior of pure FEL under different heating rates. The peak magnitude increased with the heating rate owing to the alternation of the flow of energy measured by DSC[38, 39]. The glass transition temperature of FEL was determined as 45.9°C. Numerous approaches have been proposed to determine the solubility of a drug within a polymer in the solid state, either theoretically or practically, based on different mechanisms, and one of them is to utilize the enthalpy of fusion [38, 40-49]. The enthalpy of fusion is generally defined as the heat needed to convert a substance from the solid to the liquid state without the temperature increasing [50], and it was used to calculate the drug solubility by Theeuwes et al. based on the assumption that the dissolved drug makes no contribution to the endothermic event [46]. Therefore, by plotting the enthalpy of fusion versus the drug loading concentration, the intercept on the X-axis is be the theoretical solubility of the drug within the polymer [46]. Moreover, the DSC scan rate has been reported to affect the thermal events in several studies[38, 48], as a faster scan rate will improve the sensitivity while reducing the resolution, and *vice versa*. The enthalpy of fusion values for FEL was recorded and the values were plotted versus concentration in Figure 2b; a good linear correlation was obtained for each scan rate. Subsequently, the predicted solubility of FEL in the SOL matrix was determined as 9.2, 9.9, 6.2, and 6.3% w/w. The solubility measured at a higher scan rate is lower than the value determined at a slower scan rate, and this phenomenon is similar that reported by Gramaglia et al. [38], which is possibly because a slow scan rate provides more time for the two components to achieve complete mixing.

Figure 3 demonstrates the phase solubility of FEL in aqueous solutions with or without pre-dissolved SOL. The solubility of FEL could not be detected in either medium without pre-dissolved SOL owing to the low aqueous solubility of crystalline FEL. With increasing concentration of SOL in water, the solubility of FEL was enhanced up to 20.44 μg/mL, which is attributed to the solubilizing effect of the amphiphilic structure of SOL and the formation of drug–polymer conjugates. However, the solubility of FEL in the phosphate buffer with SOL was comparatively lower than the solubility in water. Moreover, the particle size analysis of the blank SOL solution demonstrated that SOL can form micelles in both water and phosphate buffer with diameters in the range of 70–80 nm, and the particle size of the micelles remained constant when SOL concentration was above 10 μg/mL, which is consistent with the fact that the critical micelle concentration of SOL in water at 37°C was reported as 7.9 μg/mL [37] (Table 10). Interestingly, with the addition of FEL, the particle size was significantly reduced to 60-70 nm with a very narrow particle size distribution (data not shown), indicating that FEL was embedded in the micelles. Therefore, it would not be surprising to observe a solubility enhancement with nano-sized particles, and the reduction

in the particle size is most probably owing to the intermolecular interactions, for instance, hydrogen bonding, between the two components, which can attract each other.

The dissolution profiles of the FEL-SOL solid dispersions as well as the pure FEL are shown in Figure 4a. The drug loading has a clear effect on the solubility profile, and supersaturation was generated in the formulation containing 10% FEL. The solubility of FEL was increased to approximately 12 μg/mL in 30 min following precipitation, which is possibly attributed to the metastable amorphous state of FEL in the matrix. Meanwhile, solid dispersions (SDs) with 30% and 50% FEL showed a slight solubility enhancement. It was illustrated by Friesen et al. that the physical properties of a drug substance, for instance, the melting point temperature (T_m), glass transition temperature (T_g), and LogP value, affect the drug loading in formulations [51]. If T_m/T_g is larger than 1.4 while the LogP value is less than 6, the drug would tend to recrystallize from the amorphous state and limit the drug loading to between 10 and 35% in the formulation. In this case, T_m/T_g for FEL was determined as 1.87 and the LogP value was 4.83 [52]; therefore, it is expected that only the 10% solid dispersion will demonstrate a significant enhancement of solubility. The result correlated well with the predicted solubility of felodipine within the polymer when the DSC was running at a comparatively slower scan rate, 10 or 20 °C/min, indicating the viability of this method. Formulation scientists have made great efforts to inhibit the precipitation of supersaturated drug delivery systems and maintain a sufficient period of high solubility by using many approaches; one of the most important methods is to form an intermolecular interaction with the aids of different excipients, for instance, polymers [16], surfactants [53], and cyclodextrins [54]. Typically, the precipitation of a drug from a supersaturation system consists of two steps, nucleation and the following crystal growth process [10]. It is important to point out that the dissolved drug molecules have to overcome an energy barrier, which is owing to the interfacial tension between the drug particles and the dissolution medium, to form aggregates (nucleation process), which can further grow to crystals, although the precipitation is thermodynamically driven by supersaturation. Therefore, the energy barrier provides the possibility to delay or prevent the nucleation process if it could be promoted high enough and the supersaturation could remain in the metastable state for longer time. Pharmaceutical excipients, such as polymers, have been widely employed to stabilize supersaturation systems based on the mechanism of direct interaction between polymers and drug particles, and hydrogen bonding is the one observed most frequently. The active energy is increased with the formation of hydrogen bonding, and furthermore, the polymers will compete with the drug particles to absorb on the crystals or postpone the absorption by means of a steric effect, which will finally lead to a retarded crystal growth rate [10]. Clearly, the apparent solubility of FEL in all three solid dispersions was promoted and maintained in the phosphate buffer with pre-dissolved SOL (Figure 4b). This phenomenon could be explained by the pre-dissolved SOL forming micelles itself that can embed the FEL, resulting in a further enhancement of solubility. Moreover, the pre-dissolved SOL could also form an intermolecular interaction with the dissolved FEL molecules, which can delay the precipitation process. However, the amount of pre-dissolved SOL studied here did not make a significant difference to the solubility enhancement effect.

No characteristic endothermic melting peak of FEL was observed in DSC thermograms for solid dispersions at three different ratios (data not shown), which illustrates the amorphous

state of FEL in the structure. Generally, with only a single T_g, solid dispersions are considered to be homogeneous and are expected to further benefit the physical stability of extrudates; however, exceptions have been reported [55, 56]. Therefore, it is necessary to characterize the solid dispersions by utilizing other techniques. XRD has been the technique of choice to characterize solid dispersions in the pharmaceutical industry owing to its excellent capacity to provide fingerprints and quantitative analysis of substances [57]. No crystalline peaks were detected by XRD in the solid dispersions compared to the pure FEL, indicating the possible amorphous state of the drug (Figure 5).

In crystalline materials, the molecules are regularly arranged, which usually results in various refractive indices and results in the exhibition of a vivid color when the substances are observed under polarized light. On the other hand, the molecules in amorphous substance are randomly oriented, and they have only one principle refractive index. Although cubic crystals such as sodium chloride also have the same property as amorphous substances, they rarely exist in organic materials. Therefore, the crystalline and amorphous states of substances can be differentiated by polarized light owing to the different optical properties and the absence of birefringence is strong evidence of the existence of an amorphous state [58, 59]. As shown in Figure 6b, none of the SDs exhibited birefringence as contrasted to the crystalline FEL (Figure 6a), and the same observation was also made for the 10 and 50% SDs, which confirmed the amorphous state of FEL in the formulations. In addition, the SDs were also exposed to pH 6.8 phosphate buffer and were observed to simulate the dissolution process. Interestingly, the particles of the 10% FEL solid dispersion were slightly extended with a reduction in their thickness during the period of observation (Figures 6c and 6d), which likely demonstrated that the solid dispersions had already started to dissolve into the medium, while no similar phenomenon was observed for the 30 or 50% FEL solid dispersions (data not shown). This is attributed to the apparently higher solubility of the 10% FEL solid dispersions compared to the others. In addition, as the extrudes were only exposed to small amount of dissolution medium and remained statically, this observation cannot completely represent the dissolution process, therefore, only a reduction in thickness was detected However, no difference was observed when the SDs were exposed to the phosphate buffer with pre-dissolved SOL, which could be owing to the short observation time (data not shown).

FEL is able to form hydrogen bonds as a hydrogen donor with several types of polymers containing hydrogen acceptor groups[60-63]. As mentioned before, the delay in the precipitation of the FEL solid dispersions was probably owing to the intermolecular interaction with SOL. Therefore, FT-IR and Raman spectroscopy were conducted to prove this hypothesis. Crystalline FEL demonstrated a characteristic N-H stretch peak at around 3371 cm^{-1} (Figure 7), but no N-H stretch peak was detected in the solid dispersions at all three ratios, possibly owing to the formation of a hydrogen bond with the ketone group in SOL. Raman spectroscopy has been extensively applied in pharmaceutical research for both qualitative and quantitative purposes, and it has been successfully utilized to determine hydrogen bonding [64-68]. Nollenberger et al. reported that FEL has a characteristic N-H stretch peak at 3375 cm^{-1} as well as a characteristic peak at 1639 cm^{-1} owing to the free carbonyl stretching[67]. Although the N-H stretch peak in FEL was not obvious in the Raman study here, attributed to the higher intensity of other molecular vibrations (Figure 8a), a

Raman peak shift was clearly observed in the range of 1200–1700 cm^{-1}, which is an indication of potential intermolecular interaction (Figure 8b). Therefore, a theoretical calculation of the molecular vibrations of FEL was conducted to further identify the corresponding shifted peaks, and consequently, C-H bending, N-H bending, and a combination of C-C stretching with N-H bending peak were confirmed to be associated with the 8, 7, and 5 cm^{-1} wavelength peak shifts, respectively, which is indicative of the formation of hydrogen bonding (Figure 8c).

SEM has been widely applied to characterize the solid-state properties of substances in the pharmaceutical industry owing to its high magnification and resolution [58]. The morphology of the selected samples was evaluated in SEM studies. SOL powders demonstrated spherical shapes with s mooth surfaces, which indicates the amorphous state of the polymer (Figure 9a). In contrast, pure FEL powders revealed a plate-like shape with edged surfaces, attributed to the crystalline form (Figure 9b)[26]. For the 10% FEL solid dispersion, the surface was also smooth, indicating that the FEL was in an amorphous state and uniformly distributed in the matrix. However, in the solid dispersions containing 30 and 50% FEL, few species with the features of crystal FEL were detected, which possibly contributes to the phenomenon of no significant enhancement of solubility in these two solid dispersions compared to pure FEL (Figure 9c–d). In addition, the cross-section of the rods was also investigated. There was no difference between pure SOL and 10% FEL-SOL rods, which indicates that FEL is molecularly dispersed into the matrix and the formation of a solid solution. On the contrary, few small FEL crystals were also detected in part of the 30 and 50% FELSOL rods, which is consistent with the observation of the extrudates' surfaces; these small aggregates in the extrudates might also explain the lower solubility of the 30 and 50% FEL-SOL extrudates (Figures 9e–g). This discrepancy with XRD studies was probably owing to the detection limit of XRD (5% w/w)[25].

Conclusion

The solubility of a poorly water-soluble compound, FEL, was increased by preparation of amorphous solid dispersions via hot-melt extrusion with SOL, an amphiphilic polymer. The dissolution rate was improved through two pathways: amorphous solid dispersion and further encapsulation of SOL micelles. Furthermore, intermolecular interactions were determined by FT-IR and Raman spectroscopy. In addition, a solid solution was achieved for 10% FEL; however, small crystalline residues were detected for the 30 and 50% FEL-SOL extrudates by SEM. Indeed, SEM demonstrates promise for examining the distribution of active ingredients within a polymer matrix.

Acknowledgments

Declaration of Interest

The authors would like to thank the Pii Center for Pharmaceutical Technology and Grant Number P20GM104932 from the National Institute of General Medical Sciences (NIGMS), a component of NIH for contributions to this project.

References

1. Van de Waterbeemd, H.; Lennernäs, H.; Artursson, P. Drug Bioavailability: Estimation of Solubility, Permeability, Absorption and Bioavailability. Wiley-VCH Verlag GmbH & Co. KGaA; Weinheim: 2004.
2. Beak IH, Kim MS. Improved supersaturation and oral absorption of dutasteride by amorphous solid dispersions. Chem Pharm Bull (Tokyo). 2012; 60(11):1468–73. [PubMed: 23124571]
3. Van den Mooter G. The use of amorphous solid dispersions: A formulation strategy to overcome poor solubility and dissolution rate. Drug Discov Today Technol. 2012; 9(2):e79–w85.
4. Sinha S, Ali M, Baboota S, Ahuja A, Kumar A, Ali J. Solid Dispersion as an Approach for Bioavailability Enhancement of Poorly Water-Soluble Drug Ritonavir. AAPS PharmSciTech. 2010; 11(2):518–527. [PubMed: 20238187]
5. Modi A, Tayade P. Enhancement of dissolution profile by solid dispersion (kneading) technique. AAPS PharmSciTech. 2006; 7(3):87–92. [PubMed: 17233539]
6. Kanaze FI, Kokkalou E, Niopas I, Georgarakis M, Stergiou A, Bikiaris D. Dissolution enhancement of flavonoids by solid dispersion in PVP and PEG matrixes: A comparative study. J Appl Polym Sci. 2006; 102(1):460–71.
7. Greco K, Bogner R. Solution-mediated phase transformation: significance during dissolution and implications for bioavailability. J Pharm Sci. 2012; 101(9):2996–3018. [PubMed: 22213419]
8. Murphy D, Rodriguez-Cintron F, Langevin B, Kelly RC, Rodriguez-Hornedo N. Solution-mediated phase transformation of anhydrous to dihydrate carbamazepine and the effect of lattice disorder. International journal of pharmaceutics. 2002; 246(1-2):121–34. [PubMed: 12270615]
9. Cardew PT, Davey RJ. The Kinetics of Solvent-Mediated Phase Transformations. Proc. R. Soc. Lond. A. 1815; 1985398:415–428.
10. Brouwers J, Brewster ME, Augustijns P. Supersaturating drug delivery systems: the answer to solubility-limited oral bioavailability? J Pharm Sci. 2009; 98(8):2549–72. [PubMed: 19373886]
11. Urbanetz NA. Stabilization of solid dispersions of nimodipine and polyethylene glycol 2000. Eur J Pharm Sci. 2006; 28(1-2):67–76. [PubMed: 16472995]
12. Qian F, Wang J, Hartley R, Tao J, Haddadin R, Mathias N, Hussain M. Solution behavior of PVP-VA and HPMC-AS-based amorphous solid dispersions and their bioavailability implications. Pharm Res. 2012; 29(10):2765–76. [PubMed: 22315020]
13. Warren DB, Benameur H, Porter CJ, Pouton CW. Using polymeric precipitation inhibitors to improve the absorption of poorly water-soluble drugs: A mechanistic basis for utility. J Drug Target. 2010; 18(10):704–31. [PubMed: 20973755]
14. Bevernage J, Forier T, Brouwers J, Tack J, Annaert P, Augustijns P. Excipient-mediated supersaturation stabilization in human intestinal fluids. Mol Pharm. 2011; 8(2):564–70. [PubMed: 21268663]
15. Brewster ME, Vandecruys R, Verreck G, Peeters J. Supersaturating drug delivery systems: effect of hydrophilic cyclodextrins and other excipients on the formation and stabilization of supersaturated drug solutions. Pharmazie. 2008; 63(3):217–20. [PubMed: 18444510]
16. Raghavan SL, Kiepfer B, Davis AF, Kazarian SG, Hadgraft J. Membrane transport of hydrocortisone acetate from supersaturated solutions; the role of polymers. International journal of pharmaceutics. 2001; 221(1-2):95–105. [PubMed: 11397571]
17. Repka MA, Shah S, Lu J, Maddineni S, Morott J, Patwardhan K, Mohammed NN. Melt extrusion: process to product. Expert Opin Drug Deliv. 2012; 9(1):105–25. [PubMed: 22145932]
18. Breitenbach J. Melt extrusion: from process to drug delivery technology. Eur J Pharm Biopharm. 2002; 54(2):107–17. [PubMed: 12191680]
19. Miller DA, McConville JT, Yang W, Williams RO 3rd, McGinity JW. Hot-melt extrusion for enhanced delivery of drug particles. J Pharm Sci. 2007; 96(2):361–76. [PubMed: 17075869]
20. Paudel A, Worku ZA, Meeus J, Guns S, Van den Mooter G. Manufacturing of solid dispersions of poorly water soluble drugs by spray drying: Formulation and process considerations. International journal of pharmaceutics. 2012; 453(1):253–84. [PubMed: 22820134]

21. Betageri GV, Makarla KR. Enhancement of dissolution of glyburide by solid dispersion and lyophilization techniques. International journal of pharmaceutics. 1995; 126(1-2):155–160.
22. He X, Pei L, Tong HH, Zheng Y. Comparison of spray freeze drying and the solvent evaporation method for preparing solid dispersions of baicalein with Pluronic F68 to improve dissolution and oral bioavailability. AAPS PharmSciTech. 2011; 12(1):104–13. [PubMed: 21181514]
23. Hancock BC, York P, Rowe RC. The use of solubility parameters in pharmaceutical dosage form design. International journal of pharmaceutics. 1997; 1481-21
24. Van Krevelen, DW.; Te Nijenhuis, K. Properties of Polymers. Fourth, completely revised edition ed. Elsevier; Amsterdam: 2009.
25. Shah, N.; Sandhu, H.; Choi, DS.; Kalb, O.; Page, S.; Wyttenbach, N. Structured Development Approach for Amorphous Systems.. In: Williams, RO., III; Watts, AB.; Miller, DA., editors. Formulating Poorly Water Soluble Drugs. Vol. 267-310. Springer; New York Dordrecht Heidelberg London: 2012.
26. Mididoddi PK, Repka MA. Characterization of hot-melt extruded drug delivery systems for onychomycosis. Eur J Pharm Sci. 2007; 66(1):95–105.
27. Crowley MM, Fredersdorf A, Schroeder B, Kucera S, Prodduturi S, Repka MA, McGinity JW. The influence of guaifenesin and ketoprofen on the properties of hot-melt extruded polyethylene oxide films. Eur J Pharm Sci. 2004; 22(5):409–18. [PubMed: 15265510]
28. Greenhalgh DJ, Williams AC, Timmins P, York P. Solubility parameters as predictors of miscibility in solid dispersions. J Pharm Sci. 1999; 88(11):1182–90. [PubMed: 10564068]
29. Forster A, Hempenstall J, Tucker I, Rades T. Selection of excipients for melt extrusion with two poorly water-soluble drugs by solubility parameter calculation and thermal analysis. International journal of pharmaceutics. 2001; 226(1-2):147–61. [PubMed: 11532578]
30. Hildebrand, J.; Scott, R. Solubility of non-electrolytes. 3rd ed.. Reinhold; New York: 1950.
31. Hansen, CM. Hansen Solubility Parameters. 1st ed.. CRC Press LLC; Boca Raton, FL: 2000.
32. Hoy, KL. The Hoy tables of solubility parameters. Union Carbide Corporation; South Charleston: 1985.
33. Hoftyzer, PJ.; Van Krevelen, DW. Properties of Polymers. 2nd ed.. Elsevier; New York: 1976.
34. Reinemann DN, Wright AM, Wolfe JD, Tschumper GS, Hammer NI. Vibrational spectroscopy of N-methyliminodiacetic acid (MIDA)-protected boronate ester: examination of the B-N dative bond. J Phys Chem A. 2011; 115(24):6426–31. [PubMed: 21557585]
35. Qian F, Huang J, Hussain MA. Drug-polymer solubility and miscibility: Stability consideration and practical challenges in amorphous solid dispersion development. J Pharm Sci. 2010; 99(7):2941–7. [PubMed: 20127825]
36. Rubinstein, M.; Colby, RH. Thermodynamics of blends and solutions.. In: Rubinstein, M.; Colby, RH., editors. Polymer Physics. Vol. 137-170. Oxford University Press Inc.; New York: 2003.
37. Kolter K, Karl M, Gryczke A. Hot Melt Extrusion with BASF Pharma Polymers Extrusion Compendium (2nd.). 2012
38. Gramaglia D, Conway BR, Kett VL, Malcolm RK, Batchelor HK. High speed DSC (hyper-DSC) as a tool to measure the solubility of a drug within a solid or semi-solid matrix. International journal of pharmaceutics. 2005; 301(1-2):1–5. [PubMed: 16061335]
39. Gabbott, P. A Practical Introduction to Differential Scanning Calorimetry.. In: Gabbott, P., editor. Principles and Applications of Thermal Analysis. Blackwell Publishing Ltd; Ames, Iowa: 2008.
40. Marsac PJ, Shamblin SL, Taylor LS. Theoretical and practical approaches for prediction of drug-polymer miscibility and solubility. Pharm Res. 2006; 23(10):2417–26. [PubMed: 16933098]
41. Haddadin R, Qian F, Desikan S, Hussain M, Smith RL. Estimation of drug solubility in polymers via differential scanning calorimetry and utilization of the fox equation. Pharm Dev Technol. 2009; 14(1):18–26. [PubMed: 18825543]
42. Mahieu A, Willart JF, Dudognon E, Danede F, Descamps M. A new protocol to determine the solubility of drugs into polymer matrixes. Mol Pharm. 2013; 10(2):560–6. [PubMed: 23253068]
43. Yang M, Wang P, Suwardie H, Gogos C. Determination of acetaminophen's solubility in poly(ethylene oxide) by rheological, thermal and microscopic methods. International journal of pharmaceutics. 2011; 403(1-2):83–9. [PubMed: 20974240]

44. Oladiran GS, Batchelor HK. Determination of Flurbiprofen Solubility in a Wax-Based Matrix Using Hyperdsc, Higuchi Release Kinetics and Microscopy. Chem Eng Res Des. 2007; 85(7): 1039–1043.
45. Ahmed A, Barry BW, Williams AC, Davis AF. Penciclovir solubility in Eudragit films: a comparison of X-ray, thermal, microscopic and release rate techniques. J Pharm Biomed Anal. 2004; 34(5):945–56. [PubMed: 15019028]
46. Theeuwes F, Hussain A, Higuchi T. Quantitative analytical method for determination of drugs dispersed in polymers using differential scanning calorimetry. J Pharm Sci. 1974; 63(3):427–9. [PubMed: 4820377]
47. Jasti BR, Berner B, Zhou SL, Li X. A novel method for determination of drug solubility in polymeric matrices. J Pharm Sci. 2004; 93(8):2135–41. [PubMed: 15236460]
48. Tao J, Sun Y, Zhang GG, Yu L. Solubility of small-molecule crystals in polymers: D-mannitol in PVP, indomethacin in PVP/VA, and nifedipine in PVP/VA. Pharm Res. 2009; 26((4):855–64. [PubMed: 19052850]
49. Lu J, Shah S, Jo S, Majumdar S, Gryczke A, Kolter K, Langley N, Repka MA. Investigation of phase diagrams and physical stability of drug-polymer solid dispersions. Pharm Dev Technol. 2015; 20(1):105–17. [PubMed: 25113671]
50. Atkins, P.; De Paula, J. Physical Chemistry. 8th ed.. Oxford University Press; Oxford: 2009.
51. Friesen DT, Shanker R, Crew M, Smithey DT, Curatolo WJ, Nightingale JA. Hydroxypropyl methylcellulose acetate succinate-based spray-dried dispersions: an overview. Mol Pharm. 2008; 5(6):1003–19. [PubMed: 19040386]
52. Rosenbaum, SE. Basic Pharmacokinetics and Pharmacodynamics: An Integrated Textbook and Computer Simulations. 1st ed.. John Wiley & Sons, Inc.; Hoboken: 2011.
53. Rangel-Yagui CO, Pessoa A Jr. Tavares LC. Micellar solubilization of drugs. J Pharm Pharm Sci. 2005; 8(2):147–65. [PubMed: 16124926]
54. Loftsson T, Masson M, Brewster ME. Self-association of cyclodextrins and cyclodextrin complexes. J Pharm Sci. 2004; 93(5):1091–9. [PubMed: 15067686]
55. Newman A, Engers D, Bates S, Ivanisevic I, Kelly RC, Zografi G. Characterization of amorphous API:Polymer mixtures using X-ray powder diffraction. J Pharm Sci. 2008; 97(11):4840–56. [PubMed: 18351626]
56. Qian F, Huang J, Zhu Q, Haddadin R, Gawel J, Garmise R, Hussain M. Is a distinctive single Tg a reliable indicator for the homogeneity of amorphous solid dispersion? Int J Pharm. 2010; 395(1-2): 232–5. [PubMed: 20562003]
57. Gilmore, CJ. X-Ray Diffraction.. In: Storey, RA.; Ymen, I., editors. Solid State Characterization of Pharmaceuticals. John Wiley & Sons; Chichester, UK: 2011.
58. Nichols, G.; Luk, S.; Roberts, C. Microscopy.. In: Storey, RA.; Ymen, I., editors. Solid State Characterization of Pharmaceuticals. First ed.. John Wiley & Sons; Chichester, UK: 2011.
59. Hifiker, R. Polymorphism: in the Pharmaceutical Industry. Wiley-VCH Verlag GmbH & Co. KGaA; Weinheim: 2006.
60. Marsac PJ, Rumondor AC, Nivens DE, Kestur US, Stanciu L, Taylor LS. Effect of temperature and moisture on the miscibility of amorphous dispersions of felodipine and poly(vinyl pyrrolidone). J Pharm Sci. 2010; 99(1):169–85. [PubMed: 19492305]
61. Karavas E, Ktistis G, Xenakis A, Georgarakis E. Effect of hydrogen bonding interactions on the release mechanism of felodipine from nanodispersions with polyvinylpyrrolidone. Eur J Pharm Sci. 2006; 63(2):103–14.
62. Konno H, Taylor LS. Influence of different polymers on the crystallization tendency of molecularly dispersed amorphous felodipine. J Pharm Sci. 2006; 95(12):2692–705. [PubMed: 16892209]
63. Teberekidis VI, Sigalas MP. Theoretical study of hydrogen bond interactions of felodipine with polyvinylpyrrolidone and polyethyleneglycol. J Mol Struct: THEOCHEM. 2007; 803(1-3):29–38.
64. Saerens L, Dierickx L, Lenain B, Vervaet C, Remon JP, De Beer T. Raman spectroscopy for the in-line polymer-drug quantification and solid state characterization during a pharmaceutical hot- melt extrusion process. Eur J Pharm Sci. 2011; 77(1):158–63.

65. Tumuluri VS, Kemper MS, Lewis IR, Prodduturi S, Majumdar S, Avery BA, Repka MA. Off-line and on-line measurements of drug-loaded hot-melt extruded films using Raman spectroscopy. International journal of pharmaceutics. 2008; 357(1-2):77–84. [PubMed: 18316165]

66. Taylor LS, Zografi G. Spectroscopic characterization of interactions between PVP and indomethacin in amorphous molecular dispersions. Pharm Res. 1997; 14(12):1691–8. [PubMed: 9453055]

67. Nollenberger K, Gryczke A, Meier C, Dressman J, Schmidt MU, Bruhne S. Pair distribution function X-ray analysis explains dissolution characteristics of felodipine melt extrusion products. J Pharm Sci. 2009; 98(4):1476–86. [PubMed: 18752290]

68. Triggs NE, Valentini JJ. An investigation of hydrogen bonding in amides using Raman spectroscopy. J Phys Chem. 1992; 96(17):6922–31.

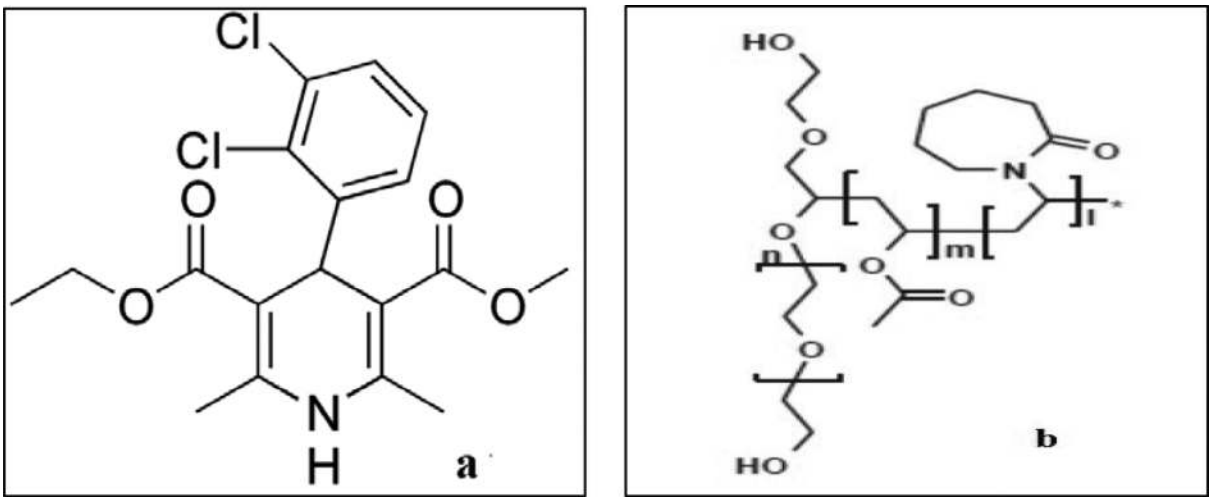

Figure 1.
a) Structure of Felodipine, b) structure of Soluplus®

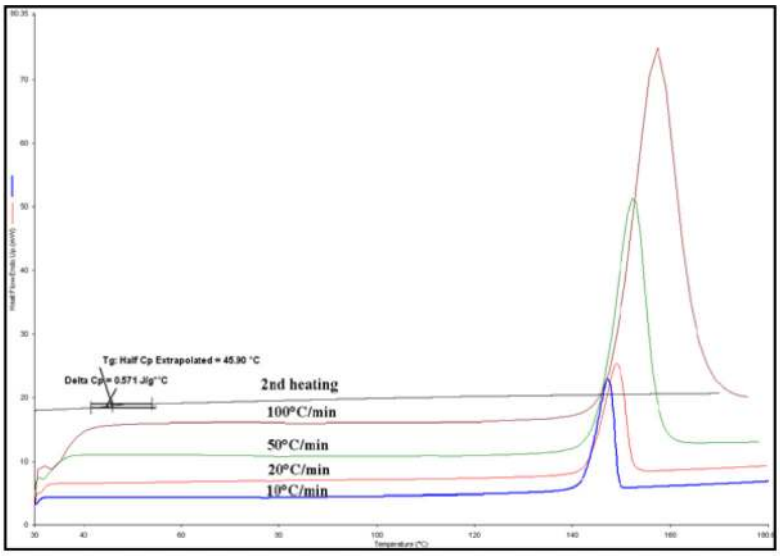

a.

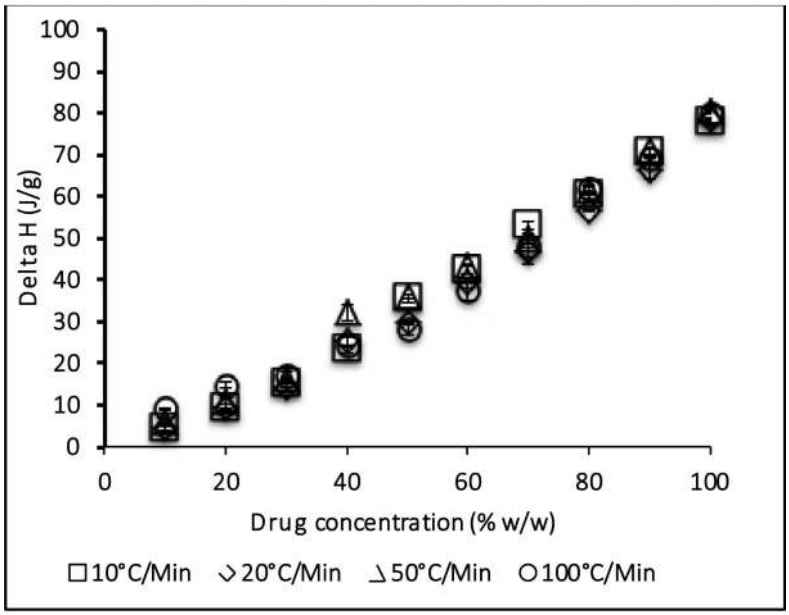

b.

Figure 2.

a) Thermograms of felodipine at different heating rates, b) Plot of Δ_H versus concentration at different heating rates

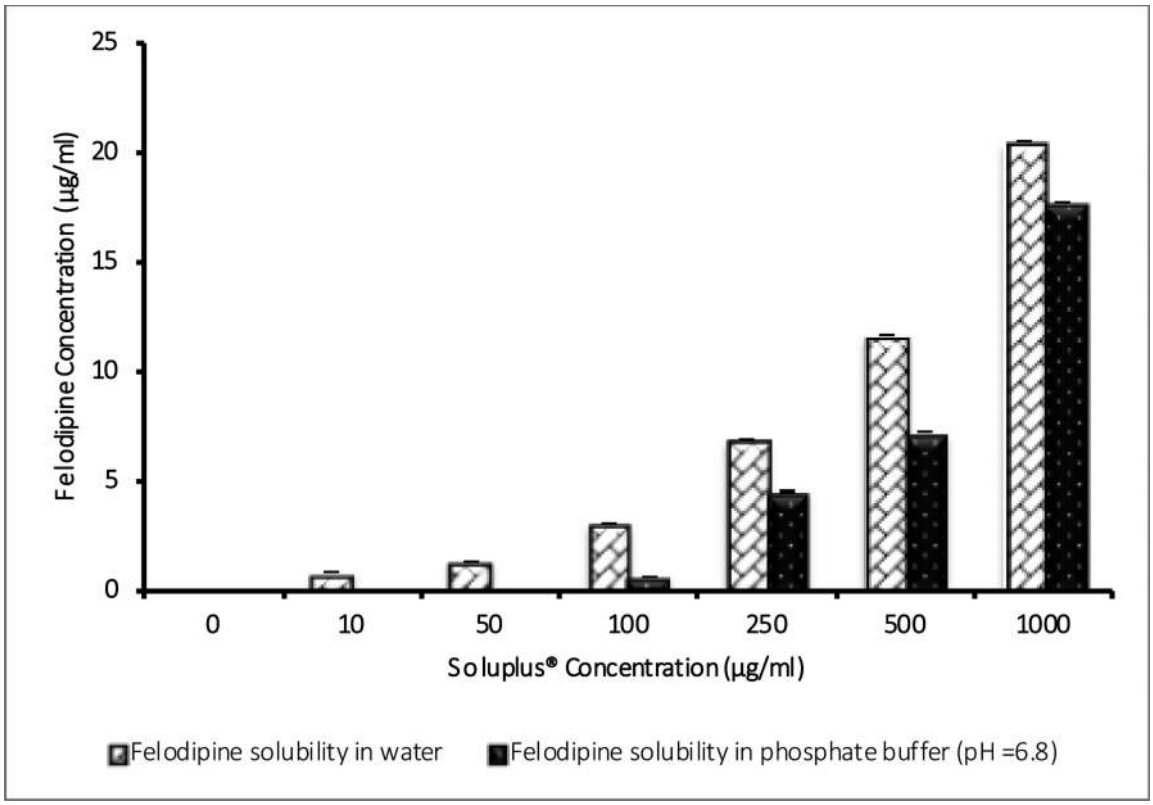

Figure 3.
Phase solubility of felodipine in aqueous solutions

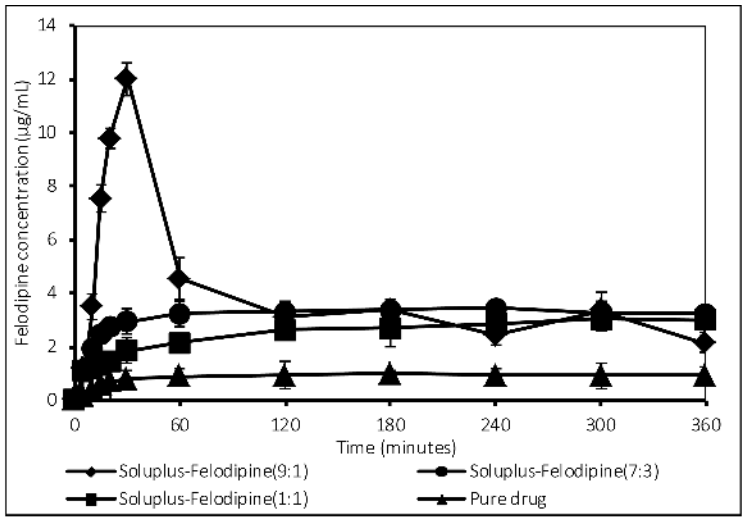

a.

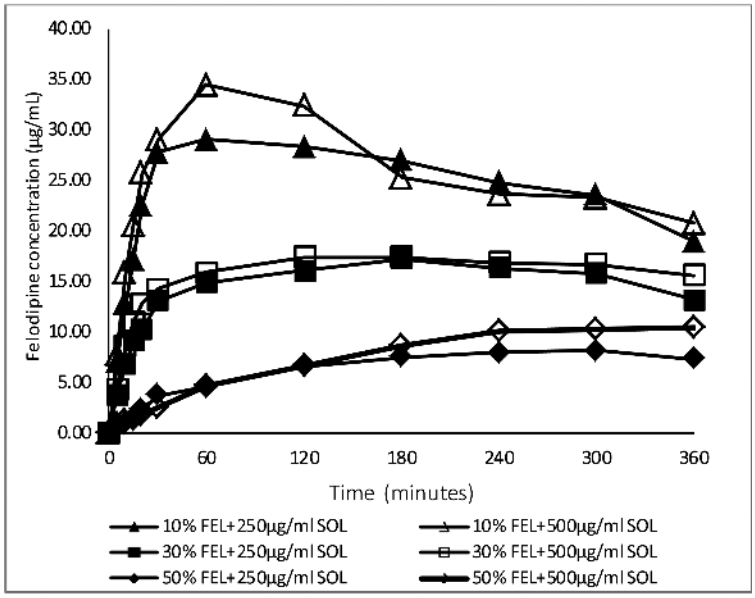

b.

Figure 4.

a) Dissolution of solid dispersions in phosphate buffer, b) Dissolution of solid dispersions in phosphate buffer with pre-dissolved Soluplus®

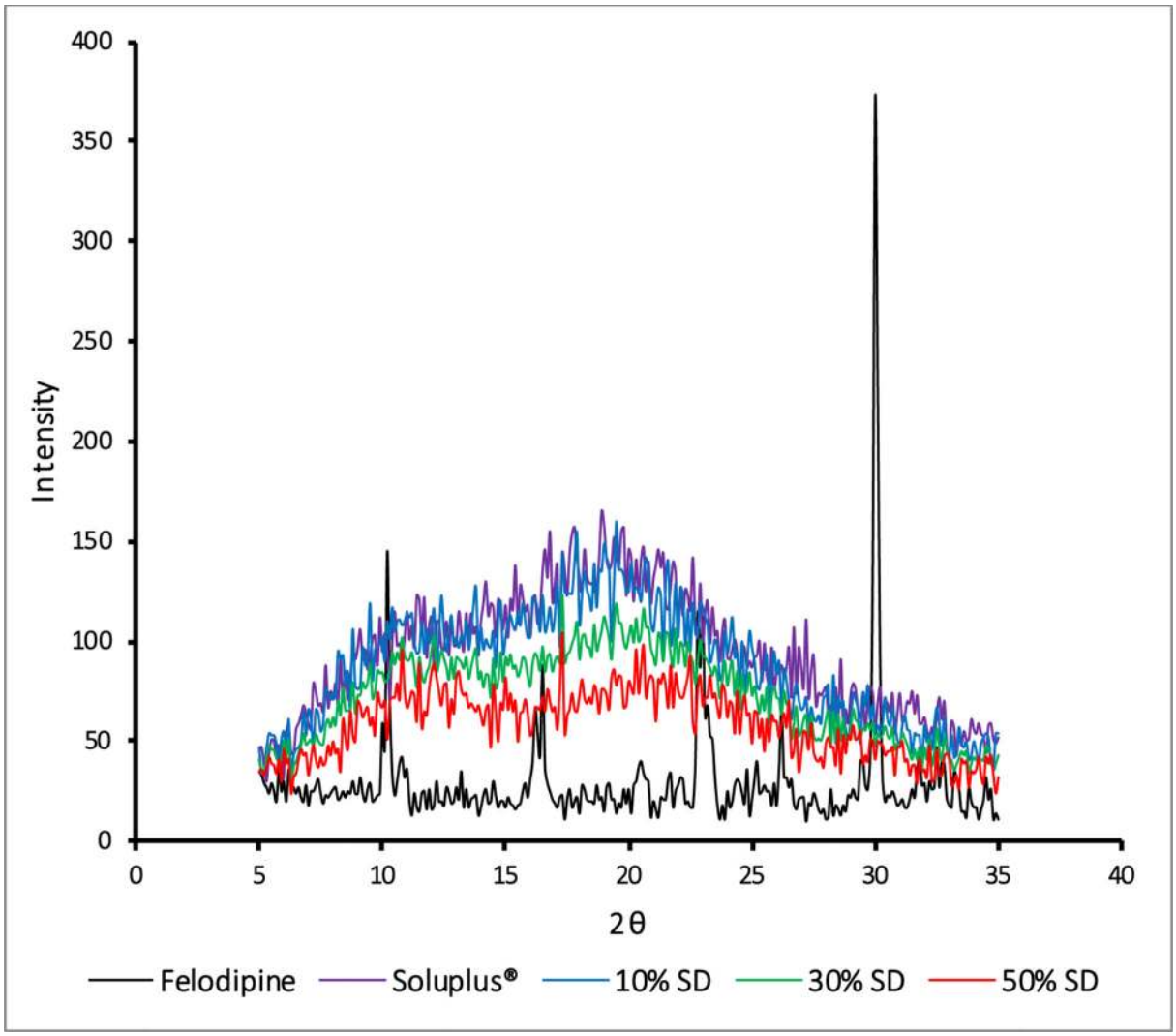

Figure 5.
X-ray diffraction plot for felodipine, Soluplus® and solid dispersions

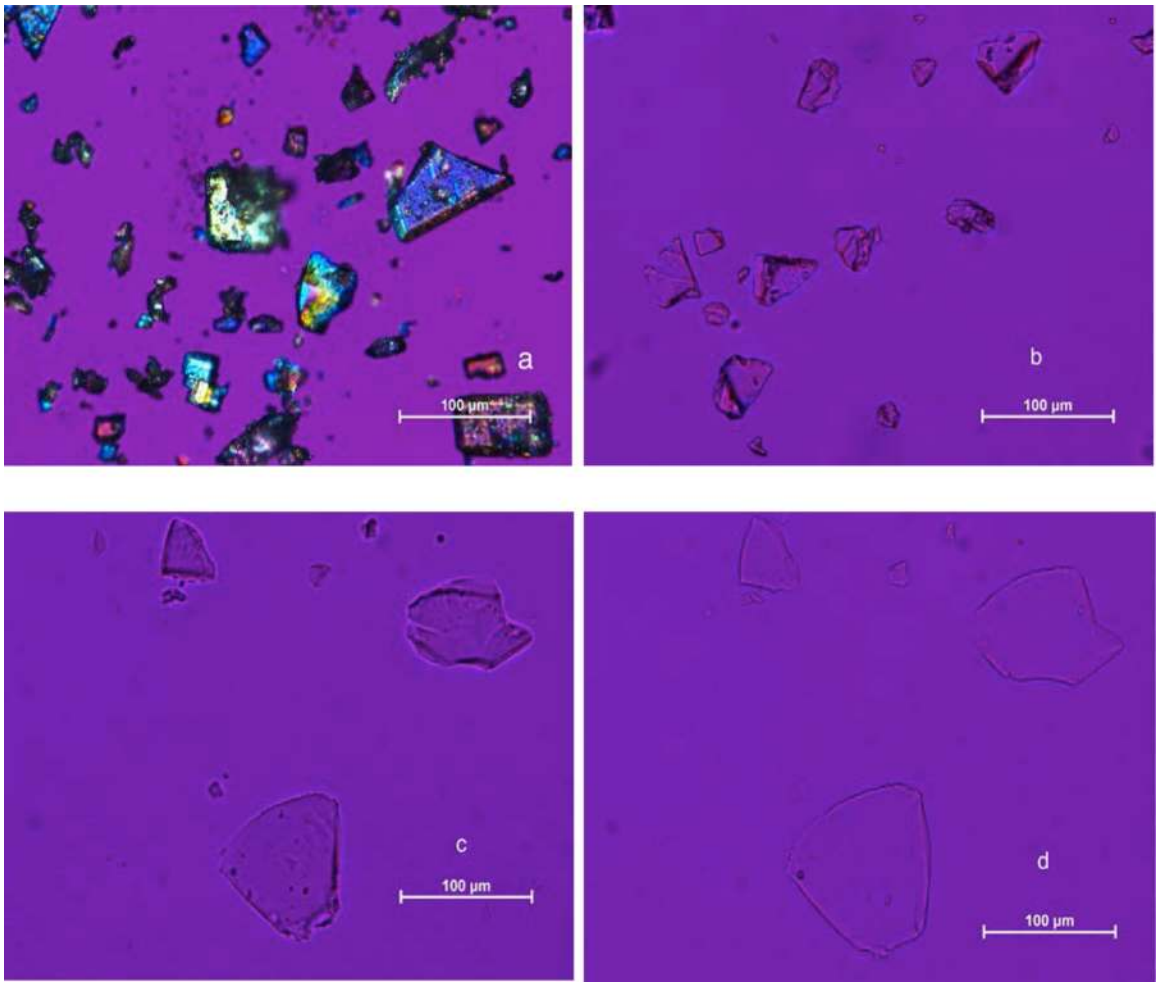

Figure 6.
Polarized light microscopy images of: (a) crystalline FEL, (b) 30% FEL-SOL solid dispersion, (c) FEL-SOL solid dispersion exposed to phosphate buffer at 0 min, and (d) 10% FEL-SOL solid dispersion exposed to phosphate buffer at 30 min.

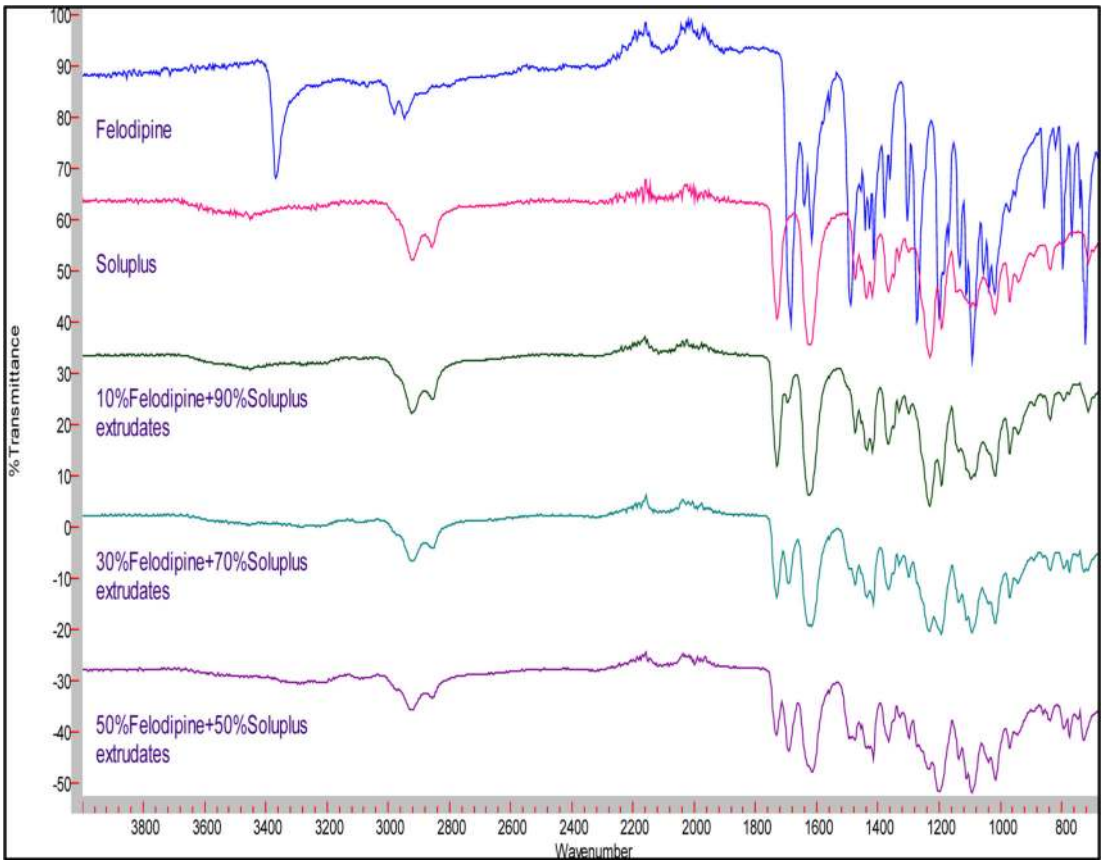

Figure 7.
FT-IR spectra of felodipine, Soluplus®, and solid dispersions

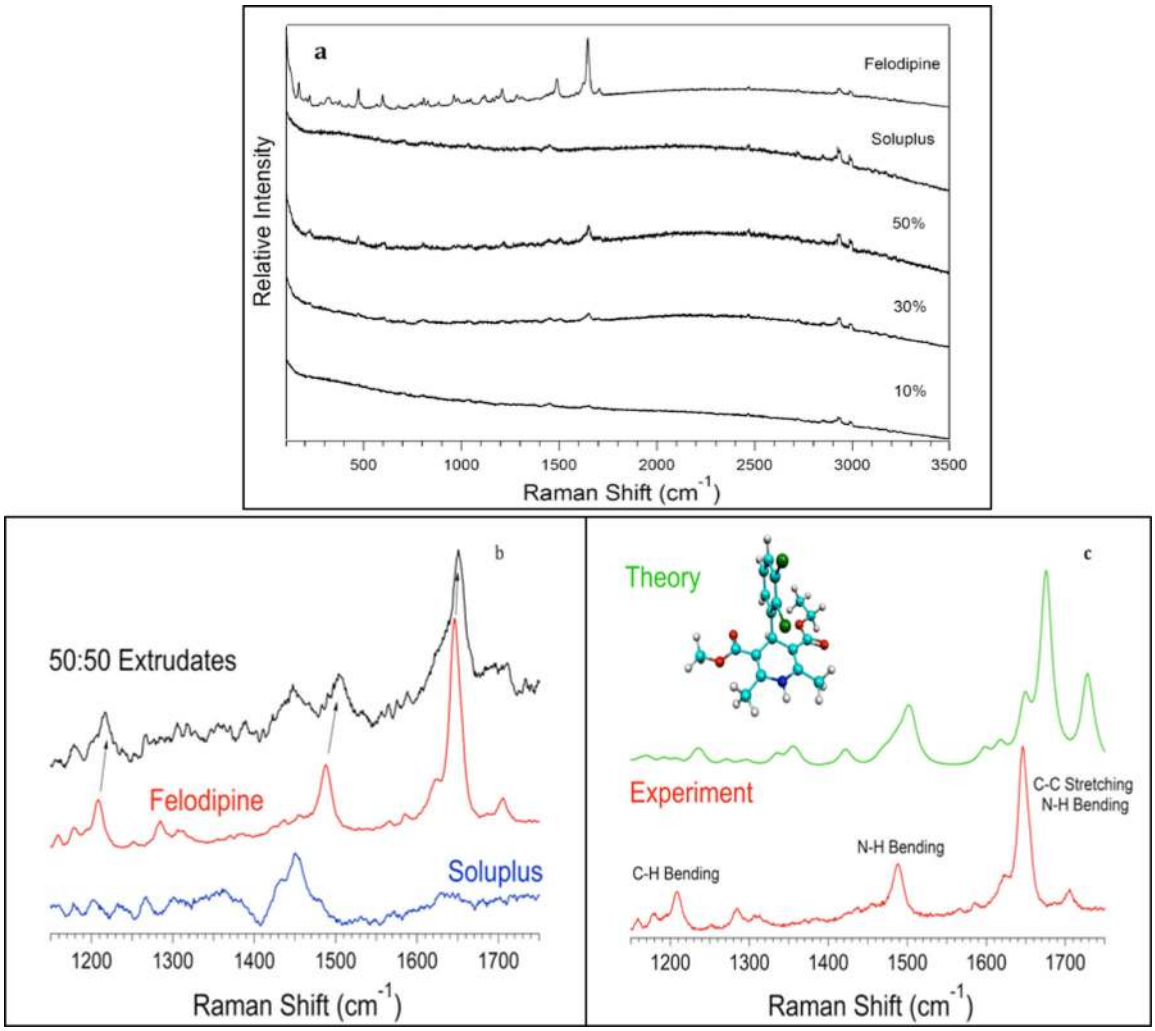

Figure 8.

a) Raman spectra of felodipine, Soluplus®, and SDs in the range of 50–3600 cm^{-1}, b) Raman spectra of FEL, SOL, and 50% FEL-SOL SD in the range of 1200–1700 cm^{-1} c) Theoretical and practical Raman spectra of FEL in the range of 1200–1700 cm^{-1}.

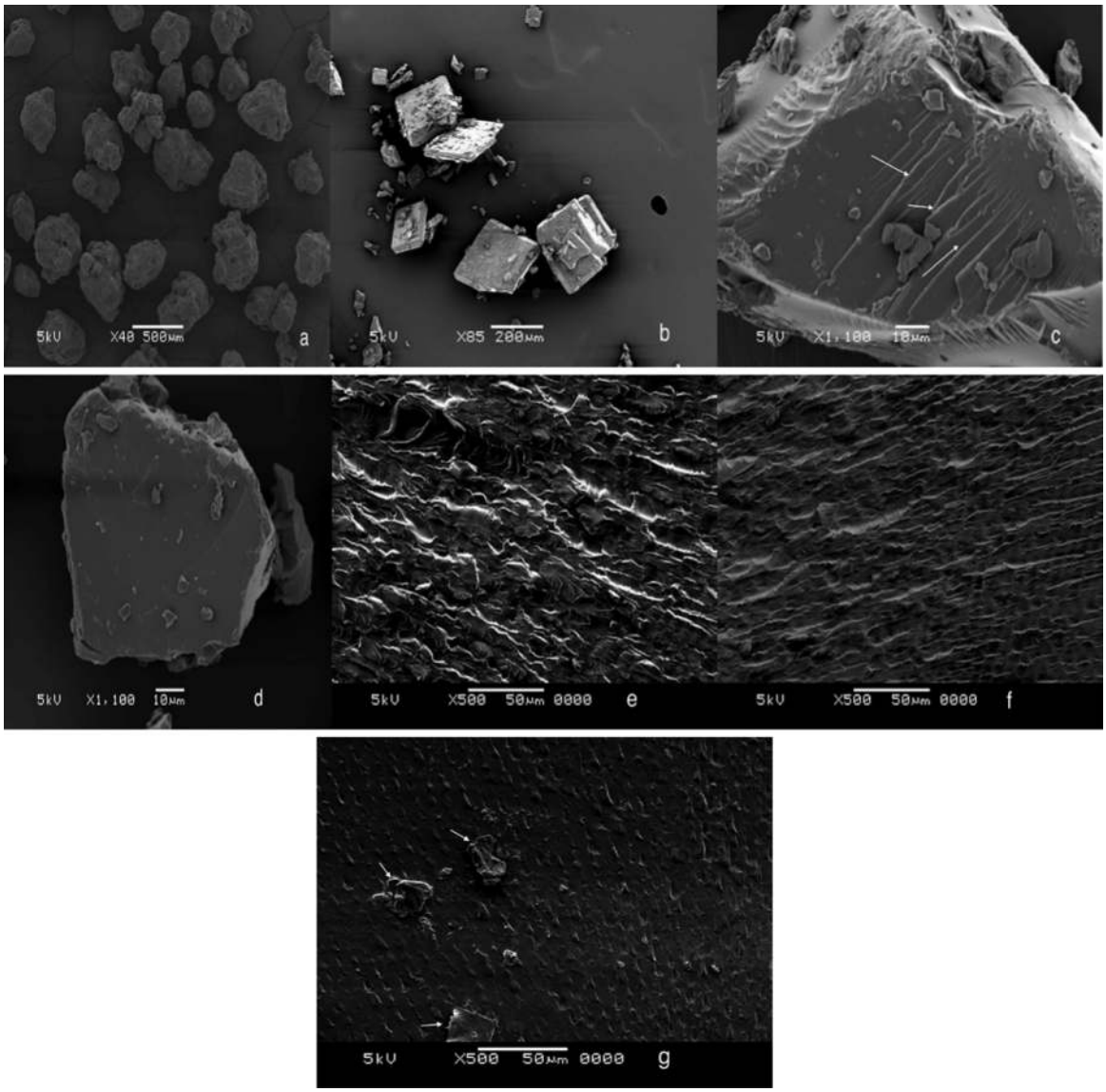

Figure 9.

Scanning electron microscopy images of: (a) SOL (b) FEL, (c) crystalline features of 30% SD, (d) smooth surface of 50% SD, (e) cross-section of SOL rods, (f) cross-section of 10% FEL-SOL rods, and (g) cross-section of 30% FEL-SOL rods.

Table 1

Group contribution of felodipine using the Hoftyzer–Van Krevelen method

Structure group	No.	F_{di} $(MJ/m^3)^{1/2}$ mol^{-1}	F_{pi} $(MJ/m^3)^{1/2}$ mol^{-1}	E_{hi} (J/mol)	V (cm^3 mol^{-1})
–CH_3	4	420	0	0	33.5
–CH_2–	1	270	0	0	16.1
>CH–	1	80	0	0	−1
=C<	4	70	0	0	−5.5
–Cl	2	450	550	400	26
–COO–	2	390	490	7000	18
–NH–	1	160	210	3100	4.5
Ring	1	190	0	0	16
Phenylene (o, m, p)	1	1270	110	0	33.4

Table 2

Group contribution of felodipine using the Hoy method

Structure group	No.	$F_{T,i}$ $(MJ/m^3)^{½}$ mol^{-1}	$\Delta_{T,i}$ $^{(P)}$	V (cm^3 mol^{-1})
–CH_3	4	303.5	0.023	21.55
–CH_2–	1	269	0.02	15.55
>CH–	1	176	0.012	9.56
=C<	4	173	0	7.18
–Cl	2	330	0.017	19.5
–COO–	2	640	0.047	23.7
–NH–	1	368	0.031	11
Ring (six membered)	1	–48	0	----
Phenylene (o, m, p)	1	20.2	0	----
$CH_{ar.}$	3	241	0.011	13.42
$C_{ar.}$	3	201	0.011	7.42

Table 3

Group contribution of PEG6000 using the Hoftyzer–Van Krevelen method

Structure group	No.	F_{di} $(MJ/m^3)^{½}$ mol^{-1}	F_{pi} $(MJ/m^3)^{½}$ mol^{-1}	E_{hi} (J/mol)	V (cm^3 mol^{-1})
–CH_2–	2	270	0	0	16.1
–OH–	2	210	500	20000	10

Table 4

Group contribution of vinyl acetate using the Hoftyzer–Van Krevelen method

Structure group	No.	F_{di} $(MJ/m^3)^{1/2}$ *mol^{-1}	F_{pi} $(MJ/m^3)^{1/2}$ *mol^{-1}	E_{hi} (J/mol)	V (cm^3 *mol^{-1})
$-CH_3$	1	420	0	0	33.5
$-COO-$	1	390	490	7000	18
$=CH-$	1	200	0	0	13.5
$=CH_2$	1	400	0	0	28.5

Table 5

Group contribution of vinyl caprolactam using the Hoftyzer–Van Krevelen method

Structure group	No.	F_{di} $(MJ/m^3)^{½}$ mol^{-1}	F_{pi} $(MJ/m^3)^{½}$ mol^{-1}	E_{hi} (J/mol)	V (cm^3 mol^{-1})
>N–	1	20	800	5000	−9
–CO–	1	290	770	2000	10.8
=CH–	1	200	0	0	13.5
$=CH_2$	1	400	0	0	28.5
$–CH_2–$	5	270	0	0	16.1
Ring	1	190	---	---	16

Table 6

Group contribution of PEG6000 using the Hoy method

Structure group	No.	$F_{T,i}$ $(MJ/m^3)^{½}$ mol^{-1}	$\Delta_{T,i}^{(P)}$	V (cm^3 mol^{-1})
–CH_2–	2	269	0.02	15.55
–OH–	2	675	0.049	12.45

Table 7

Group contribution of vinyl acetate using the Hoy method

Structure group	No.	$F_{T,i}$ $(MJ/m^3)^{1/2}$ mol^{-1}	$\Delta_{T,i}$ $^{(P)}$	V (cm^3 mol^{-1})
–CH_3	1	303.5	0.022	21.55
–COO–	1	640	0.05	23.7
=CH–	1	249	0.0185	13.18
=CH_2	1	259	0.018	19.17

Table 8

Group contribution of vinyl caprolactam using the Hoy method

Structure group	No.	$F_{T,i}$ $(MJ/m^3)^{1/2}$ mol^{-1}	$\Delta_{T,i}^{(P)}$	V (cm^3 mol^{-1})
>N–	1	125	0.008	12.14
–CO–	1	538	0.04	17.3
=CH–	1	249	0.0185	13.18
$=CH_2$	1	259	0.018	19.17
$–CH_2–$	5	269	0.02	15.55
Ring (seven membered)	1	92	0.007	---

Table 9

Summary of the calculated parameters of felodipine, monomers, and Soluplus®

	FEL	PVC	PVA	PEG	SOL
Hoy	20.78	19.45	19.48	35.08	21.49
Hoftyzer–Van Krevelen	22.74	20.43	18.16	36.14	21.79
Average	21.76	---	---	---	21.64

Table 10

Particle size analysis (mean ± standard deviation, diameter in nm). Solution A: phosphate buffer with Soluplus®; solution B: water with Soluplus®; solution C: felodipine in phosphate buffer with Soluplus®; solution D: felodipine in water with Soluplus®.

Concentration of Soluplus® (μg/mL)	Solution A	Solution B	Solution C	Solution D
0	---	---	---	---
10	78.75 ± 1.23	67.12 ± 1.31	65.32 ± 1.65	62.29 ± 2.01
50	78.98 ± 2.19	62.89 ± 1.45	67.58 ± 2.01	62.17 ± 1.98
100	73.47 ± 1.87	64.30 ± 1.21	67.19 ± 1.11	61.16 ± 1.78
250	70.74 ± 2.23	65.25 ± 1.63	66.60 ± 1.32	61.56 ± 1.89
500	71.25 ± 0.98	63.06 ± 1.99	63.30 ± 1.47	60.87 ± 1.45
1000	72.29 ± 1.34	63.17 ± 1.12	62.80 ± 1.32	60.98 ± 1.89